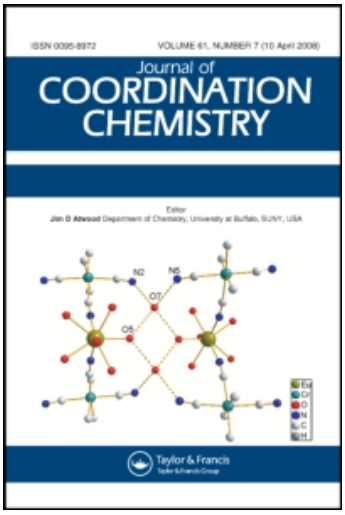

Journal of Coordination Chemistry
Publication details, including instructions for authors and subscription information:
http://www.informaworld.com/smpp/title~content=t713455674

Synthesis, crystal structure, and luminescence properties of $[TbGd(NAA)_6(phen)_2]$ and $[Tb_2(NNA)_6(phen)_2] \cdot 2C_3H_7NO$

Yu-Fen Liu[a]; De-Fu Rong[b]; Hai-Tao Xia[a]; Da-Qi Wang[c]; Liang Chen[a]
[a] School of Chemical Engineering, Huaihai Institute of Technology, Lianyungang, P.R. China [b] Beilun Entry-Exit Inspection and Quarantine Bureau of China, Zhejiang, P.R. China [c] College of Chemistry and Chemical Engineering, Liaocheng University, Shandong, P.R. China

First published on: 29 July 2010

To cite this Article Liu, Yu-Fen , Rong, De-Fu , Xia, Hai-Tao , Wang, Da-Qi and Chen, Liang(2009) 'Synthesis, crystal structure, and luminescence properties of $[TbGd(NAA)_6(phen)_2]$ and $[Tb_2(NNA)_6(phen)_2] \cdot 2C_3H_7NO$', Journal of Coordination Chemistry, 62: 11, 1835 — 1845, First published on: 29 July 2010 (iFirst)
To link to this Article: DOI: 10.1080/00958970802691440
URL: http://dx.doi.org/10.1080/00958970802691440

Journal of Coordination Chemistry
Vol. 62, No. 11, 1 June 2009, 1835–1845

Synthesis, crystal structure, and luminescence properties of $[TbGd(NAA)_6(phen)_2]$ and $[Tb_2(NNA)_6(phen)_2]\cdot 2C_3H_7NO$

YU-FEN LIU*†, DE-FU RONG‡, HAI-TAO XIA†, DA-QI WANG§ and LIANG CHEN†

†School of Chemical Engineering, Huaihai Institute of Technology, Lianyungang, P.R. China
‡Beilun Entry-Exit Inspection and Quarantine Bureau of China, Zhejiang, P.R. China
§College of Chemistry and Chemical Engineering, Liaocheng University, Shandong, P.R. China

(*Received 12 March 2008; in final form 4 September 2008*)

Lanthanide(III) heteronuclear and binuclear complexes $[TbGd(NAA)_6(phen)_2]$ (**1**) and $[Tb_2(NAA)_6(phen)_2]\cdot 2C_3H_7NO$ (**2**) (NAA = 1-naphthylacetic acid, phen = 1,10-phenanthroline) were prepared and their crystal structures were determined. In **1** and **2**, each lanthanide is nine-coordinate by two bidentate-bridging and two tridentate chelating-bridging carboxylate groups, one bidentate chelating carboxylate and one phen molecule in a distorted monocapped square antiprism. The solid-state luminescence behavior and the antibacterial activities were studied. Complexes **1** and **2** exhibited characteristic emission of Tb(III) ion $^5D_4 \rightarrow {}^7F_J$ ($J = 6$–0) under UV radiation at room temperature. A main excitation peak (359 nm) of **2** appears under red emission of 615 nm. By contrast, all emission peak intensities of **1** were enhanced by addition of gadolinium(III), and the 545 nm band is much stronger than the 615 nm band, attributed to, under perturbation of the ligand field, the probability of $^5D_4 \rightarrow {}^7F_3$ transition of Tb(III) was greatly enhanced in **2**. Because of perturbation of the ligand field by addition of gadolinium(III), the probability of $^5D_4 \rightarrow {}^7F_5$ transition of Tb(III) was greatly enhanced in **1** and green fluorescence was observed. The antibacterial activity showed that the two complexes were active against *Escherichia coli*, *Staphylococcus aureus* and *Bacillus subtilis*.

Keywords: Lanthanide; 1-Naphthylacetic acid; Crystal structure; Fluorescence; 1,10-Phenanthroline

1. Introduction

Effort has been focused on rare earth aromatic carboxylate complexes due to their interesting structural diversities, variable coordination number and potential applications in fields [1, 2] such as luminescence, magnetic, and electroluminescent materials. Many rare earth complexes with fluorescence have been synthesized and the crystal structures of some complexes were studied [3–22]. The coordination number of rare

*Corresponding author. Email: liu222005@hhit.edu.cn

Journal of Coordination Chemistry
ISSN 0095-8972 print/ISSN 1029-0389 online © 2009 Taylor & Francis
DOI: 10.1080/00958970802691440

earth ions is from 7 to 9 since they have different ionic radii and electronic configurations [23]. Generally, a negative organic ligand acts as the first ligand to the central ion while a neutral secondary ligand saturates the rare earth coordination number and also improves the fluorescence intensity and stability [18]. Fluorescence enhancement of rare earth complexes can also occur through addition of certain rare earth ions [20]. Previously, we reported the crystal structure of **2** [21]. As part of our studies on the structure and luminescence of lanthanide aromatic carboxylates, a new heteronuclear complex $[TbGd(NAA)_6(phen)_2]$ (NAA = 1-naphthylacetic acid, phen = 1,10-phenanthroline) was synthesized and characterized by crystal structure, solid-state fluorescence properties, and antibacterial activity. The emission peak intensities of **1** were enhanced by addition of gadolinium(III) due to the energy level and the structure.

2. Experimental

2.1. *Materials*

All starting materials were of reagent chemical grade. The solvents used in the physical measurements were of analytical reagent grade.

2.2. *Preparation of complexes (1) and (2)*

To a stirred solution of NAA (0.559 g, 3 mmol) and phen (phenmonohydrate (0.198 g, 1 mmol) in 30 mL methanol, a solution of $Tb(NO_3)_3 \cdot 6H_2O$ (0.227 g, 0.5 mmol) and $Gd(NO_3)_3 \cdot 6H_2O$ (0.226 g, 0.5 mmol) in water (10 mL) was added. The mixed solution was heated to 333–343 K and stirred for 3 h. The precipitate was then filtered, washed with water and ethanol, and dried to afford colorless powder in 81.1% (0.981 g) yield; recrystallization of **1** from *N,N′*-dimethylformamide at room temperature gave crystals suitable for X-ray single crystal diffraction analysis. Anal. Calcd for $C_{96}H_{70}N_4O_{12}TbGd$ (1787.73): C, 64.44; H, 3.92; N, 3.13%. Found: C, 64.59; H, 3.87; N, 3.09%. The infrared (IR) spectrum exhibits a pattern of bands in the range 4000–400 cm^{-1}: 1560 cm^{-1} ($\nu_{as}COO^-$); 1424 cm^{-1} (ν_sCOO^-).

Complex **2** was prepared in the same process except adding the second lanthanide Gd(III) ions, yield is 78.6% (0.951 g). Anal. Calcd for $C_{102}H_{84}N_6O_{14}Tb_2$ (1935.59): C, 63.24; H, 4.34; N, 4.34%. Found: C, 63.29; H, 4.26; N, 4.31%. IR (KBr, cm^{-1}): 1562 ($\nu_{as}COO^-$); 1425 cm^{-1} (ν_sCOO^-).

2.3. *Physical measurements*

Elemental analysis was measured by a Perkin–Elmer 2400c Element analyzer. IR spectra were recorded on a Nicolet 5DX FT-IR spectrophotometer using KBr discs in the range 4000–400 cm^{-1}. Solid-state excitation and emission spectra were obtained with an FL3-TCSPC spectrophotometer. Spectra were recorded using monochromator slit widths of 1 nm on both excitation and emission sides at room temperature.

2.4. *X-ray crystal structure determination*

Colorless single crystals of **1** and **2** suitable for X-ray crystallographic analysis were mounted on sealed glass capillaries. Diffraction data were collected with a Bruker SMART 1000 CCD diffractometer by use of graphite monochromated Mo-Kα radiation ($\lambda = 0.71073$ Å) at 298(2) K. The crystal structure was solved by direct methods and all nonhydrogen atoms were located with successive difference Fourier syntheses. The structure was refined by full-matrix least-squares on F^2 with anisotropic thermal parameters for all non-hydrogen atoms. The hydrogen atoms were added according to theoretical models. The NAA bridged to Tb1 (Gd1) were disordered over two sites. The coordinates of these two sites were refined with the occupancies tied to sum to unity, the site occupancies for C2–C12 with attached H atoms and C2′–C12′ with attached H atoms refined to 0.612(15) and 0.388(15), respectively. All calculations were performed using programs contained in SHELXL [24, 25]. A summary of crystallographic data and refinement parameters for **1** and **2** are given in table 1.

2.5. *Antimicrobial activity determination*

The test of antimicrobial activity adopts a method of agar diffusion [26] using DMF as the solvent. The antimicrobial activity of the NAA, phen, and two complexes were obtained with different concentrations. Culture medium of antibiotic medium consists of beef extract, albumens, and agars. The culture medium, experimental apparatus, and filter paper of 5 mm diameter were sterilized for 30 min at 120°C; the culture medium

Table 1. Crystal data and structure refinement for **1** and **2**.

Complex	**1**	**2**
Formula	$C_{96}H_{70}N_4O_{12}TbGd$	$C_{102}H_{84}N_6O_{14}Tb_2$
Formula weight	1787.73	1935.59
Temperature (K)	298(2)	298(2)
Wavelength (Å)	0.71073	0.71073
Radiation	Mo-Kα	Mo-Kα
Crystal system	Triclinic	Monoclinic
Space group	$P\bar{1}$	$P2_1/c$
Unitcells and dimensions (Å, °)		
a	12.0509(14)	13.4619(16)
b	12.4065(15)	15.086(2)
c	15.013(2)	22.166(2)
α	76.284(3)	90
β	74.524(3)	103.584(2)
γ	66.266(2)	90
V (Å^3)	1958.8(4)	4375.6(9)
Z	1	2
D_{Calcd} (mg m^{-3})	1.516	1.469
$F(000)$	899	1960
Crystal size (mm^3)	$0.32 \times 0.20 \times 0.12$	$0.28 \times 0.17 \times 0.12$
θ Range for data collection (°)	1.42–25.01	1.56–25.01
Reflections collected/unique (R_{int})	9865/6760 (0.0276)	22392/7671 (0.1971)
Refinement method	Full-matrix least-squares on F^2	Full-matrix least-squares on F^2
Data/restraints/parameters	6760/0/608	7671/0/559
Goodness-of-fit on F^2	1.019	1.068
Final R indices [$I > 2\sigma(I)$]	$R_1 = 0.0482$, $wR_2 = 0.1211$	$R_1 = 0.0763$, $wR_2 = 0.1577$
Largest difference peak and hole (e Å^{-3})	2.567 and −0.956	2.747 and −2.675

was transferred to glass plates and froze at 37°C. After *Escherichia coli*, *Staphylococcus aureus*, and *Bacillus subtilis* were inoculated to the solid culture medium surface, the filter paper with 10 μL samples were placed on the surface. They were allowed to incubate at 37°C for 18 h. The inhibition zone around the disc was calculated as zone diameter in millimeters. Blank tests showed that DMF in the preparation of the test solutions does not affect the test organisms. All tests were repeated three times and average data were taken as the final result.

3. Results and discussion

3.1. *Crystal structure of (1)*

Results of single crystal X-ray diffraction show that the crystal structures of **1** and **2** are isomorphous, crystallizing in the triclinic space group $P\bar{1}$ and monoclinic space group $P2_1/c$, respectively. The molecular structure of **1** is shown in figure 1. Selected bond lengths and angles are listed in table 2.

Complex **1** is centrosymmetric with equal disorder of the Tb and Gd atoms. The central Tb and Gd atoms are both nine-coordinate by seven oxygens and two nitrogens. The carboxylate groups are bonded to Tb(III) or Gd(III) as bidentate chelating, bidentate bridging, and tridentate chelating-bridging. Each Tb(III) or Gd(III) ion is coordinated to one bidentate chelating carboxylate, two bidentate bridging, and two

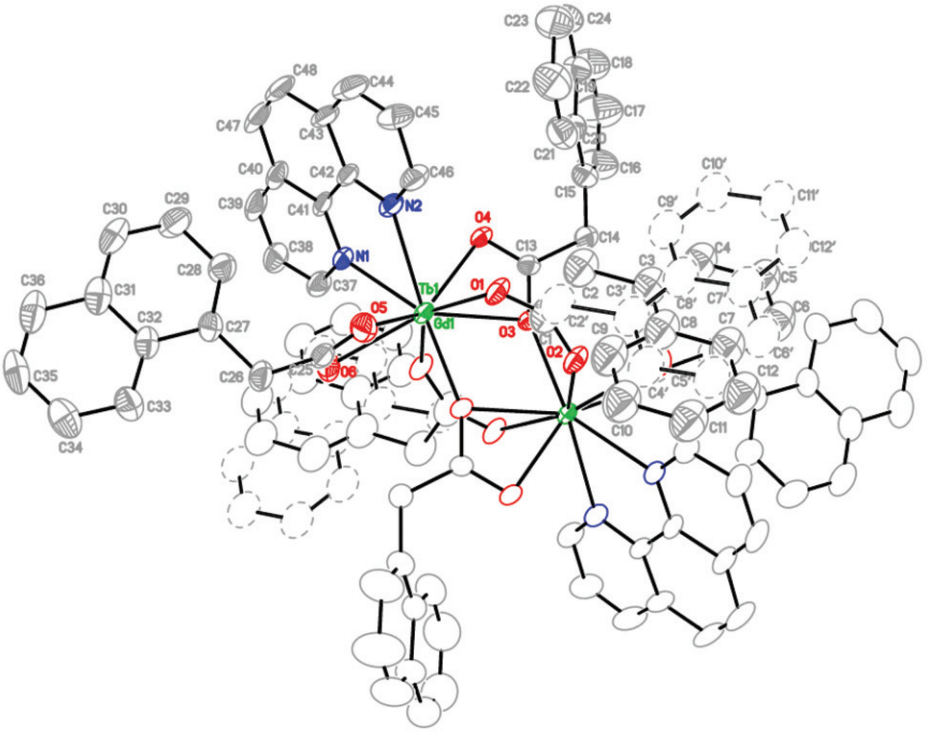

Figure 1. Molecular structure of $[TbGd(NAA)_6(phen)_2]$.

tridentate chelating-bridging carboxylates, as well as one phen. The coordination geometry can be described as a distorted monocapped square antiprism, the oxygen from the tridentate chelating-bridging carboxylate is at the capped position.

The Tb(Gd)–O bond distances are all different, ranging from 2.336(9) to 2.556(5) Å. The Tb(Gd)–O bonds formed by the tridentate chelating-bridging carboxylates are slightly longer than that formed by the bidentate chelating carboxylate except

Table 2. Selected bond lengths (Å) and angles (°) for **1** and **2**.

Complex **1**		Complex **2**	
Tb1(Gd1)–O3^{i}	2.336(4)	Tb1–O1^{ii}	2.343(5)
Tb1(Gd1)–O1	2.362(5)	Tb1–O1	2.539(7)
Tb1(Gd1)–O2^{i}	2.372(5)	Tb1–O2	2.478(7)
Tb1(Gd1)–O6	2.429(5)	Tb1–O6	2.433(8)
Tb1(Gd1)–O5	2.470(6)	Tb1–O5	2.468(8)
Tb1(Gd1)–O4	2.483(5)	Tb1–O4^{ii}	2.369(7)
Tb1(Gd1)–O3	2.556(5)	Tb1–O3	2.349(6)
Tb1(Gd1)–N1	2.592(6)	Tb1–N1	2.587(7)
Tb1(Gd1)–N2	2.605(6)	Tb1–N2	2.547(9)
Tb–Gd1^{i}	3.9290(8)	Tb1–Tb1^{ii}	3.9302(9)
O3^{i}–Tb1(Gd1)–O1	75.27(17)	O1^{ii}–Tb1–O3	74.6(2)
O3^{i}–Tb1(Gd1)–O2^{i}	76.73(17)	O3–Tb1–O2	77.0(2)
O1–Tb1(Gd1)–O2^{i}	136.93(17)	O1^{ii}–Tb1–O2	123.5(2)
O3^{i}–Tb1(Gd1)–O6	81.15(18)	O3–Tb1–O6	125.4(3)
O1–Tb1(Gd1)–O6	127.10(2)	O1^{ii}–Tb1–O6	86.6(2)
O2^{i}–Tb1(Gd1)–O6	79.10(2)	O6–Tb1–O2	148.4(2)
O3^{i}–Tb1(Gd1)–O5	81.02(19)	O3–Tb1–O5	72.9(2)
O1–Tb1(Gd1)–O5	76.50(2)	O1^{ii}–Tb1–O5	75.6(2)
O2^{i}–Tb1(Gd1)–O5	129.87(19)	O2–Tb1–O5	137.8(3)
O6–Tb1(Gd1)–O5	53.20(2)	O6–Tb1–O5	52.7(3)
O3^{i}–Tb1(Gd1)–O4	124.57(16)	O3–Tb1–O4^{i}	136.6(2)
O1–Tb1(Gd1)–O4	82.20(19)	O1^{ii}–Tb1–O4^{ii}	76.8(2)
O2^{i}–Tb1(Gd1)–O4	87.53(19)	O4^{ii}–Tb1–O2	92.8(2)
O6–Tb1(Gd1)–O4	147.51(19)	O4^{ii}–Tb1–O6	84.2(3)
O5–Tb1(Gd1)–O4	140.92(19)	O4^{ii}–Tb1–O5	129.4(3)
O3^{i}–Tb1(Gd1)–O3	73.21(17)	O1^{ii}–Tb1–O1	72.8(3)
O1–Tb1(Gd1)–O3	69.32(17)	O1–Tb1–O3	68.8(2)
O2^{i}–Tb1(Gd1)–O3	71.63(17)	O2–Tb1–O1	51.5(2)
O6–Tb1(Gd1)–O3	144.62(19)	O6–Tb1–O1	151.3(3)
O5–Tb1(Gd1)–O3	141.25(18)	O5–Tb1–O1	135.3(2)
O4–Tb1(Gd1)–O3	51.44(15)	O4–Tb1–O1	72.0(2)
O3^{i}–Tb1(Gd1)–N1	144.92(18)	O3–Tb1–N1	137.0(3)
O1–Tb1(Gd1)–N1	138.88(18)	O1^{ii}–Tb1–N1	148.4(3)
O2^{i}–Tb1(Gd1)–N1	77.71(18)	O2–Tb1–N1	73.5(2)
O6–Tb1(Gd1)–N1	70.73(19)	O6–Tb1–N1	75.2(3)
O5–Tb1(Gd1)–N1	97.60(2)	O5–Tb1–N1	110.9(3)
O4–Tb1(Gd1)–N1	77.56(17)	O4^{ii}–Tb1–N1	75.8(3)
O3–Tb1(Gd1)–N1	120.07(17)	O1–Tb1–N1	112.7(2)
O3^{i}–Tb1(Gd1)–N2	144.49(19)	O1^{ii}–Tb1–N2	142.4(2)
O1–Tb1(Gd1)–N2	76.46(19)	O1–Tb1–N2	120.3(3)
O2^{i}–Tb1(Gd1)–N2	138.58(19)	O2–Tb1–N2	73.8(3)
O6–Tb1(Gd1)–N2	99.5(2)	O6–Tb1–N2	88.3(3)
O5–Tb1(Gd1)–N2	71.82(19)	O5–Tb1–N2	71.7(3)
O4–Tb1(Gd1)–N2	71.54(18)	O4^{ii}–Tb1–N2	139.6(2)
O3–Tb1(Gd1)–N2	115.56(17)	O3–Tb1–N2	78.3(2)
O1–C1–O2	128.3(8)	O1–C1–O2	122.4(10)
O4–C13–O3	119.5(6)	O4–C13–O3	126.5(9)
O5–C25–O6	122.1(8)	O5–C25–O6	122.5(11)

Symmetry codes: (i) $-x+2$, $-y+2$, $-z+2$. (ii) $-x+1$, $-y+1$, $-z+2$.

for Tb–O3^{i}. The Tb–Gd distances are 3.9290(8) Å. The bond lengths of Tb(Gd)–N are 2.592(6) and 2.605(6) Å. Different coordination modes cause different O–C–O angles. The O–C–O angles [128.3(8)°] of the bidentate bridging carboxylate is the largest, the O–C–O angle [122.1(8)°] of the bidentate chelating carboxylate is second, and the O–C–O angle [119.5(6)°] of tridentate chelating-bridging carboxylate group is the smallest. The dihedral angles between the least-square plane Tb_2O_2 (Gd_2O_2) and naphthyl rings are 22.54(69)° (C3–C12 ring), 57.22(19)° (C15–C24 ring), 18.38(22)° (C27–C36 ring), and the dihedral angle between Tb_2O_2 or Gd_2O_2 plane and phen ring is 87.34(9)°. The one NAA ligand bridged to Tb1 (Gd1) is disordered over two sites, the site occupancies for C2–C12 and C2′–C12′ ring with attached H atoms refined to 0.612(15) and 0.388(15), respectively.

Figure 2 shows the packing view of a unit cell for **1**. There are five C–H $\cdots$ O and two C–H $\cdots\pi$ intermolecular hydrogen bonds in the structure of **1**. All those hydrogen bonds link complex units, resulting in a three-dimensional network. The detailed data of hydrogen bonds for **1** are shown in table 3.

Complex **2** is similar in structure to **1**. The Tb–O1^{i} bond distance is 2.343(5) Å, longer than the Tb(Gd)–O1^{i} [2.336(4) Å] of **1**, and the Tb–O1 bond [2.539(7) Å] is shorter than the Tb(Gd)–O1 [2.556(5) Å] because the radius of the Gd ion is greater than the Tb ion. The Tb–Tb distance in **2** is 3.9302(9) Å, slightly longer than the metal–metal

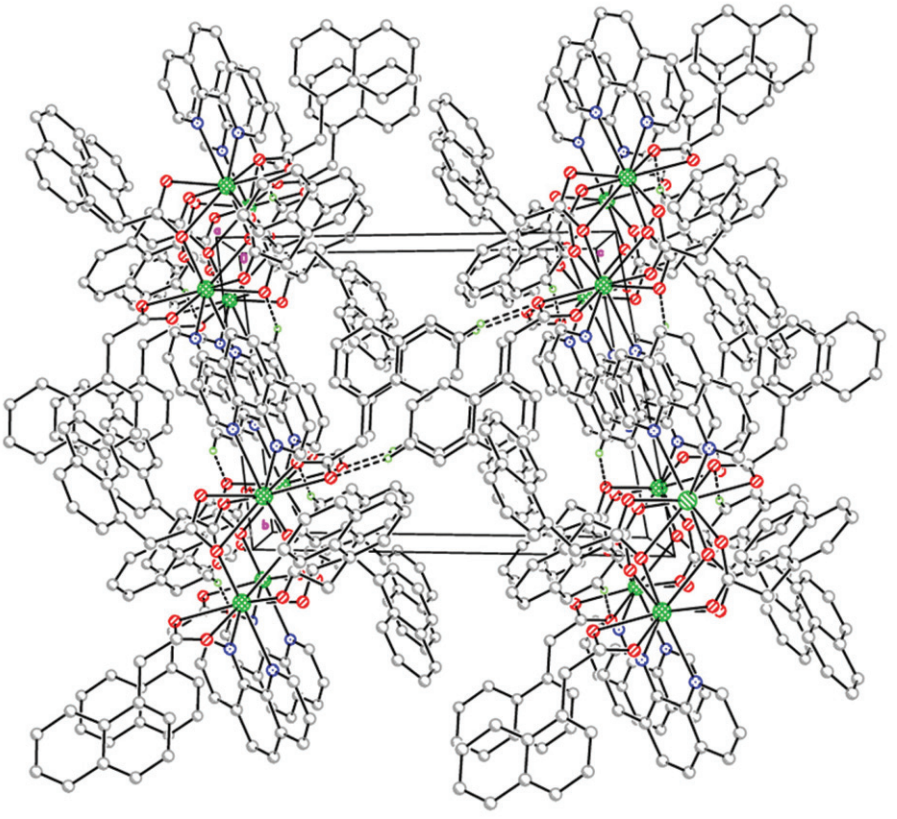

Figure 2. Packing view of the unit cell for [TbGd(NAA)$_6$(phen)$_2$].

distance in **1**. The Tb–N bond distances are in the range 2.547(9)–2.587(7) Å, smaller than the Tb(Gd)–N bond distances in **1**.

3.2. *IR spectra*

Infrared spectra of free ligand, **1** and **2** were determined in KBr matrix from 4000 to 400 cm^{-1}. The IR spectra for complexes are similar, showing their structures are similar. The band of COOH group for NAA at 1689 cm^{-1} disappears in spectra of the complexes. The asymmetric and symmetric stretching vibrations of carboxylate in **1** and **2** are at 1560, 1562 and 1424, 1422 cm^{-1}. The splitting of the vibration bands of carboxylate indicate that the COO^- groups function in different coordination fashions [19], confirmed by X-ray diffraction analysis. The C–H stretching vibrations at 837 and 729 cm^{-1} in phen shift to 842 and 727 cm^{-1} in **1** and 842, 722 cm^{-1} in **2**, indicating bonds are formed between lanthanide and nitrogen of phen [5].

3.3. *Antimicrobial activity*

From data in table 4, the complexes and ligand exhibit antibacterial activity against all test bacteria. The two complexes show higher activity compared to NAA. The antibacterial activities of **1** are almost the same for *E. coli*, and *S. aureus* at 1.04×10^{-3}, 4.16×10^{-3} mol L^{-1}. The antibacterial activities of **2** are almost the same for *E. coli*, and *B. subtilis* at 4.16×10^{-3} mol L^{-1}, indicating that antibacterial activity depends on the type of bacteria.

3.4. *Fluorescence spectra*

Excitation spectra of **1** and **2** are recorded by monitoring the Tb(III) ion luminescence at 545 and 615 nm in the range 200–500 nm. As shown in figure 3, for the complexes, the

Table 3. Hydrogen bond geometries (Å, °) for **1** and **2**.

D–H···*A*	*D*–H	H···*A*	*D*···*A*	*D*–H···*A*
Complex **1**				
C37–H37···O2^{i}	0.93	2.42	3.060(10)	126
C46–H46···O1	0.93	2.36	3.021(10)	128
C11–H11···O5^{ii}	0.93	2.46	3.37(3)	166
C47–H47···O4^{iii}	0.93	2.49	3.353(10)	155
C35–H35···O6^{iv}	0.93	2.64	3.311(13)	130
C16–H16···Cg1^{v}	0.93	2.87	3.67(3)	144
C39–H39···Cg2^{iii}	0.93	2.83	3.668(18)	151
Complex **2**				
C6–H6···O^{b}	0.93	2.56	3.44(2)	157
C37–H37···O4^{a}	0.93	2.35	3.015(11)	128
C46–H46···O3	0.93	2.48	3.056(13)	120
C47–H47···O2^{c}	0.93	2.45	3.314(13)	154
C50–H50A···O6^{d}	0.96	2.62	3.40(2)	138
C18–H18···Cg1^{e}	0.93	2.90	3.676916)	141

Symmetry codes: ^{i} $-x+2, -y+2, -z+2$; ^{ii} $-x+1, -y+2, -z+2$; ^{iii} $-x+3, -y+1, -z+2$; ^{iv} $-x+2, -y+1, -z+3$; ^{v} $x+1, y, z$. ^{a} $-x+1, -y+1, -z+2$; ^{b} $-x, -y+1, -z+1$; ^{c} $-x, -y+1, -z+2$; ^{d} $x, y, z1$; ^{e} $-x+1, y+1/2, -z+1/2$.

Table 4. The antimicrobial activity of the ligand and complexes.

	Diameter of inhibition zone (mm)								
	E. coli			*S. aureus*			*B. subtilis*		
Compound	*c*1	*c*2	*c*3	*c*1	*c*2	*c*3	*c*1	*c*2	*c*3
NAA	12.0	14.0	18.0	9.2	10.0	10.8	10.0	11.0	10.8
Phen	14.0	24.2	32.0	19.3	25.0	32.0	18.1	26.0	26.2
$[TbGd(C_{12}H_9O_2)_6(C_{12}H_8N_2)_2]$	11.0	16.2	19.0	11.5	18.0	19.0	16.0	17.5	19.0
$[Tb_2(C_{12}H_9O_2)_6(C_{12}H_8N_2)_2]\cdot 2C_3H_7NO$	14.3	24.0	22.8	15.5	27.5	26.4	17.1	20.8	22.5

$c1 = 1.04 \times 10^{-3}$ mol L^{-1}, $c2 = 2.60 \times 10^{-3}$ mol L^{-1}, $c3 = 4.16 \times 10^{-3}$ mol L^{-1}.

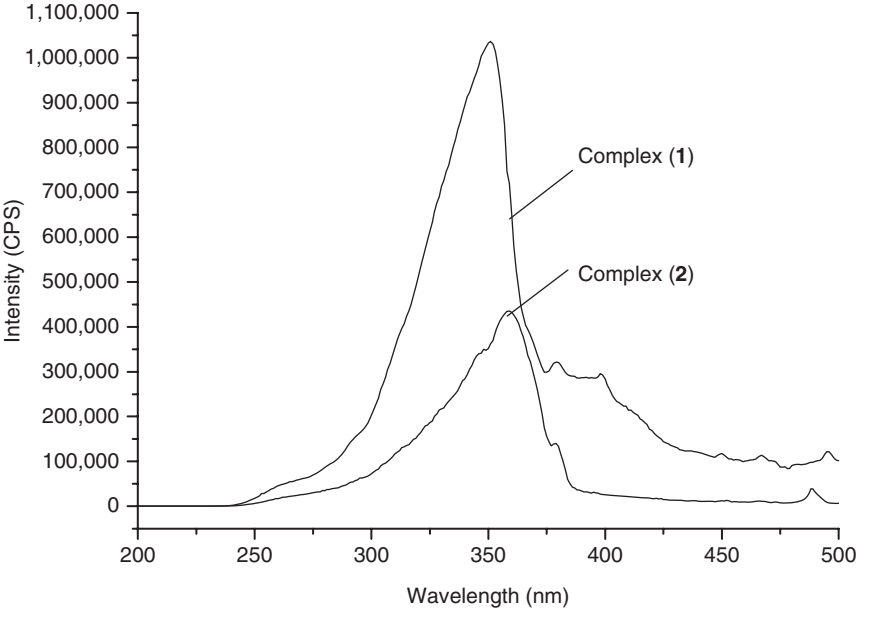

Figure 3. Excitation spectra, $\lambda_{em} = 545$, 615 nm for **1** and **2**, respectively.

broad excitation bands at 250–380 nm (the maximum excitation wavelength are 351 and 359 nm, respectively) are attributed to the $^7F_6 \rightarrow {}^5G_5$ and the $^7F_6 \rightarrow {}^5L_9$ transitions, the $^7F_6 \rightarrow {}^5D_4$ and the $^7F_6 \rightarrow {}^5D_3$, $^5G_6$ and $^5L_{10}$ transitions are at 495 (490 nm for **2**) and 380 nm, respectively. The positions of their excitation bands are similar. However, compared with **2**, the excitation band of **1** is broadened and blue shifted, and its intensity increases dramatically.

Emission spectra were recorded from 400–700 nm by monitoring the maximum excitation wavelength. As shown in figure 4, complex crystals produced typical band features in the wavelength region 400–700 nm, originating from the $^5D_4$ state to the ^7F_J ($J = 6$–0) transitions of Tb(III) ion. The band positions of the luminescence of **1** are almost identical to those of **2**, but band splitting of the two complexes differ. Significant differences between these two complexes can be found in the luminescence intensity.

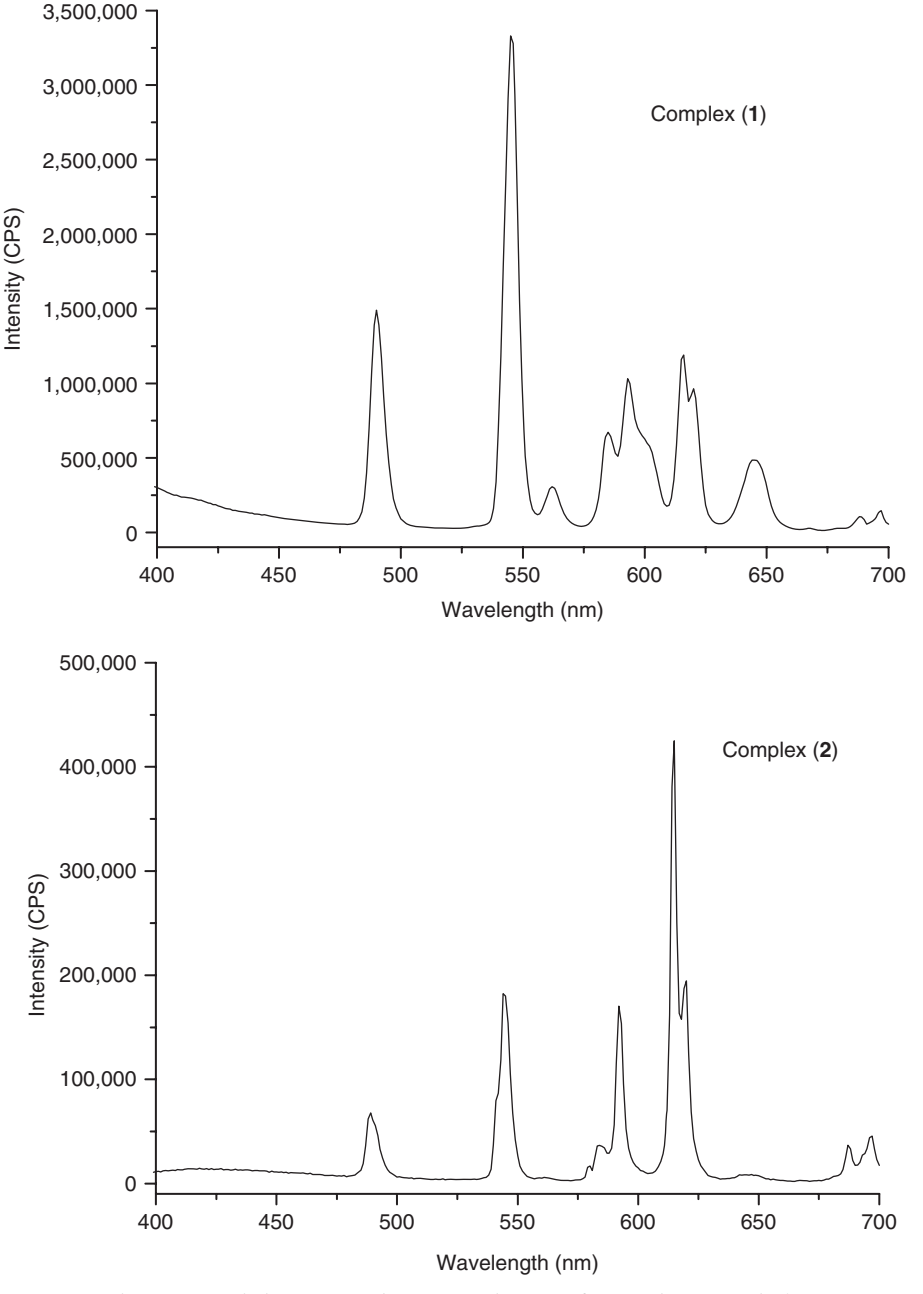

Figure 4. Emission spectra, $\lambda_{ex} = 351$ and 359 nm for **1** and **2**, respectively.

The luminescence intensity of **1** is markedly enhanced, compared with that of **2**. For **1**, the $^5D_4 \rightarrow {}^7F_2$ transition appeared with weak intensity at 645 nm, while for **2**, this transition did not appear. The medium-intensity 490, 593, and 615 nm bands are attributed to the transitions from the $^5D_4$ to $^7F_6$, $^7F_4$ and $^7F_3$ states, respectively.

These transitions show moderate sensitivity to the ligand environment. The most intense luminescence is observed in the $^5D_4 \rightarrow {}^7F_5$ transition peaking at 545 nm. This transition is the best probe transition. Other $^5D_4 \rightarrow {}^7F_{1,0}$ transitions at 687 and 697 nm, respectively, are very weak.

For **2**, the band at 615 nm is more intense than the others, consistent with the observation that the $^5D_4 \rightarrow {}^7F_3$ transition is the preferred transition of phen-2-naphthoate complex of terbium [27], which may be attributed to perturbation of the ligand field [27] and the aggregation state of particulates [28]. Therefore, the probability of $^5D_4 \rightarrow {}^7F_5$ transition of Tb(III) was greatly enhanced in **1** and green fluorescence was observed, while red fluorescence was observed for **2**. The splitting of the fluorescence peak for **1** and **2** are due to crystal-field splitting [19].

Enhancement of fluorescence of **1** by addition of Gd(III) may be concerned with both the structure of the complexes and the intramolecular energy transfer. Intramolecular energy transfer efficiency from organic ligands to lanthanide ion is the most important factor influencing the luminescence properties of lanthanide complexes. Intramolecular energy transfer efficiency depends on two energy transfer processes [16]: the first comes from the lowest triplet state of ligand to the emissive energy level of the lanthanide ion by Dexter's resonant energy transfer interaction; the second is the inverse energy transfer by a thermal deactivation mechanism. Both energy transfer rate constants depend on the energy differences between the triplet level of the ligand and the resonant emissive energy level of lanthanide ion. If the energy gap is too small or large, the efficiency of energy transfer will decrease because of a thermal de-excitation process, and luminescence intensity decreases. It is reported that thermal de-excitation is evident when the energy gap between the triplet state of the ligand and lanthanide ion is less than 1800 cm^{-1} [11]. The energy level of the triplet state of phen (22.132 cm^{-1}) is too near to the energy level of $^5D_4$ (20,500 cm^{-1}) of Tb(III) ion [6, 10], which will make the thermal de-excitation process happen easily. Thus, most of the excitation energy is consumed, leading to poor photoluminescence of **2**. The Gd(III) ions incorporated with emitting energy level higher (32.221 cm^{-1}) [18] than the triplet level of the ligand and energy cannot transfer from ligand to Gd(III). As a result, the energy absorbed by ligands coordinated with Gd(III) is transferred to the Tb(III) ions through the oxo bridges and, therefore, the luminescence intensity of **1** enhances.

4. Conclusions

We have synthesized lanthanide complexes with NAA and phen, $[TbGd(NAA)_6(phen)_2]$ and $[Tb_2(NAA)_6(phen)_2] \cdot 2C_3H_7NO$. The crystal structures and fluorescence properties were investigated. The X-ray structure confirms that the complexes have the same structure with nine-coordinate lanthanide. Under ultraviolet light excitation, the complexes exhibited characteristic luminescence of terbium, indicating that phen is a good organic chelator to absorb and transfer energy to lanthanide ions. The luminescence intensity of **1** is markedly enhanced compared with that of **2**. The band at 545 nm is more intense for **1** and the band at 615 nm is more intense for **2**. The results indicate that luminescence behavior of Tb(III) was changed by the addition of gadolinium(III) and the selection of ligands.

Supplementary materials

Crystallographic data for the structures in this article have been deposited with the Cambridge Crystallographic Data Centre as the supplementary publication CCDC No. 656137, 649518 for **1** and **2**. Copies of the data can be obtained, free of charge, on application to CCDC, 12 Union Road, Cambridge CB2 1EZ, UK.

Acknowledgment

We acknowledge the financial support of the Huaihai Institute of Technology Science Foundation.

References

[1] U.P. Singh, R. Kumar, S. Upreti. *J. Mol. Struct.*, **831**, 97 (2007).
[2] P. Gawryszewska, J. Sokolnicki, J. Legendziewicz. *Coord. Chem. Rev.*, **249**, 2489 (2005).
[3] L. Liu, Z. Xu, Z.-D. Lou, F.-J. Zhang, B. Sun, J. Pei. *J. Lumin.*, **122–123**, 961 (2007).
[4] C.-H. Ye, H.-L. Sun, X.-Y. Wang, J.-R. Li, D.-B. Nie, W.-F. Fu, S. Gao. *J. Solid State Chem.*, **177**, 3735 (2004).
[5] N. Ren, J.-J. Zhang, S.-L. Xu, R.-F. Wang, S.-P. Wang. *Thermochim. Acta*, **438**, 172 (2005).
[6] Y.-S. Song, B. Yan, Z.-X. Chen. *J. Solid State Chem.*, **177**, 3805 (2004).
[7] Y.-S. Song, B. Yan, L.-H. Weng. *Polyhedron*, **26**, 4591 (2007).
[8] B. Xu, B. Yan. *Spectrochim. Acta, Part A*, **66**, 236 (2007).
[9] J.-C. Lee, K.-S. Choi, H.-K. Cho, J.-G. Kang. *J. Lumin.*, **127**, 332 (2007).
[10] L.-M. Ruan, H. Wang, Y.-Y. Hao, H.-F. Zhou, X.-G. Liu, B.-S. Xu. *J. Lumin.*, **122–123**, 467 (2007).
[11] Y.-T. Yang, S.-Y. Zhang. *Spectrochim. Acta, Part A*, **60**, 2065 (2004).
[12] J.-G. Kang, T.-J. Kim, H.-J. Kang, S.-K. Kang. *J. Photochem. Photobiol. A: Chem.*, **174**, 28 (2005).
[13] D.-X. Hu, P.-K. Chen, F. Luo, Y.-X. Che, J. Zheng. *J. Mol. Struct.*, **837**, 179 (2007).
[14] D. Ang, G.B. Deacon, P.C. Junk, D.R. Turner. *Polyhedron*, **26**, 385 (2007).
[15] T. Ishizaka, H. Kasai, H. Oikawa, H. Nakanishi. *J. Photochem. Photobiol. A: Chem.*, **183**, 280 (2006).
[16] Y. Huang, B. Yan, M. Shao, Z.-X. Chen. *J. Mol. Struct.*, **871**, 59 (2007).
[17] X.-J. Zheng, L.-P. Jin, Z.-M. Wang, C.-H. Yan, S.-Z. Lu, Q. Li. *Polyhedron*, **22**, 323 (2003).
[18] Y. Chen, W.-M. Cai. *Spectrochim. Acta, Part A*, **62**, 863 (2005).
[19] M.-C. Yin, C.-C. Ai, L.-J. Yuan, C.-W. Wang, J.-T. Sun. *J. Mol. Struct.*, **691**, 33 (2004).
[20] C.-J. Xu, F. Xie, X.-Z. Guo, H. Yang. *Spectrochim. Acta, Part A*, **61**, 2005 (2005).
[21] H.-T. Xia, Y.-F. Liu, D.-Q. Wang, S.-P. Yang. *Acta Crystallogr., Sect. E*, **63**, m2624 (2007).
[22] Q.-S. Shi, S. Zhang, Q. Wang, H.-W. Ma, G.-Q. Yang, W.-H. Sun. *J. Mol. Struct.*, **837**, 185 (2007).
[23] N. Sakagami, J. Homma, T. Konno, K. Okamoto. *Acta Crystallogr., Sect. C*, **53**, 1376 (1997).
[24] G.M. Sheldrick. *SHELXS-97, Program of X-Ray Crystal Structure Solution*, University of Göttingen, Göttingen, Germany (1997).
[25] G.M. Sheldrick. *SHELXL-97, Program for X-Ray Crystal Structure Refinement*, University of Göttingen, Göttingen, Germany (1997).
[26] H.H. Fahmy, E.A. Masry, S.H.A. Abdelwhed. *Arch. Pharm. Res.*, **24**, 27 (2001).
[27] Y. Zhao, D.-T. Xie, J.-G. Wu, G.-Q. Yao, Z.-F. Song, G.-X. Xu. *Spectrosc. Spectral Anal. (Chinese)*, **18**, 173 (1998).
[28] X.-G. Wang, H.-Y. Wu, G.-Q. Yao, S.-F. Weng, J.-G. Wu. *Spectrosc. Spectral Anal. (Chinese)*, **24**, 708 (2004).